Lifetime reduction of surface states at Cu, Ag, and Au(111) caused by impurity scattering

Swantje Heers, Phivos Mavropoulos,[*] Samir Lounis, Rudolf Zeller, and Stefan Blügel

Peter Grünberg Institut and Institute for Advanced Simulation, Forschungszentrum Jülich and JARA, D-52425 Jülich, Germany

We present density-functional results on the lifetime of the (111) surface state of the noble metals. We consider scattering on the Fermi surface caused by impurity atoms belonging to the $3d$ and $4sp$ series. The results are analyzed with respect to film thickness and with respect to separation of scattering into bulk or into surface states. While for impurities in the surface layer the overall trends are similar to the long-known bulk-state scattering, for adatom-induced scattering we find a surprising behavior with respect to the adatom atomic number. A plateau emerges in the scattering rate of the $3d$ adatoms, instead of a peak characteristic of the d resonance. Additionally, the scattering rate of $4sp$ adatoms changes in a zigzag pattern, contrary to a smooth parabolic increase following Linde's rule that is observed in bulk. We interpret these results in terms of the weaker charge screening and of interference effects induced by the lowering of symmetry at the surface.

I. INTRODUCTION

The lifetime of the noble-metal (111) surface states has been the subject of numerous theoretical and experimental investigations. These states are formed due to the breaking of translational symmetry at the surface in combination with the band gap existing in the surface-projected band structure in the [111] direction. Due to their localized nature, they play a role in a variety of surface-related phenomena, such as catalysis, adsorbate interactions, or surface transport, and can be probed by spectroscopic surface-sensitive techniques such as scanning tunneling microscopy and spectroscopy (STM and STS, respectively), photoemission, etc.[1] They furthermore constitute the fundament for the appearance of quantum-interference phenomena such as the famous quantum mirage in quantum-coral systems.[2]

Although surface states are orthogonal to bulk states when only the periodic crystal and surface potential is considered, in reality there are always coupling mechanisms of the surface states to each other and to the bulk states. Mainly, these mechanisms are electron-electron interactions (including interactions with collective electron modes such as plasmons), henceforth labeled "ee," electron-phonon interactions, henceforth labeled "ep," but also scattering at defects of the surface such as step edges, islands or adsorbate atoms, henceforth labeled "ed." The total lifetime τ associated with these mechanisms is related to a sum of the scattering rates by

$$\frac{1}{\tau} = \frac{1}{\tau_{ee}} + \frac{1}{\tau_{ep}} + \frac{1}{\tau_{ed}}. \quad (1)$$

At low temperature, the phonon contribution becomes negligible, while the contribution of the electron-electron interaction depends on the electron energy E with respect to the Fermi level E_F.[3] For E close to E_F, and assuming Fermi-liquid behavior, the contribution to the decrease of the lifetime from electron-electron interactions behaves as $\tau_{ee}^{-1} \sim (E - E_F)^2$ and is thus also ultimately frozen out. However, the scattering at defects remains finite.

The lifetime τ of surface states is an experimentally measurable quantity. Most commonly used methods for this purpose are angular resolved photoemission spectroscopy (ARPES)[4–6] and STS.[1,7] ARPES can detect the full surface band structure, $E_{\vec{k}}$ and $\tau_{\vec{k}}$ (with $1/\tau_{\vec{k}}$ appearing as a broadening Γ of the electron bands), but defect scattering is necessarily averaged over a large surface area and cannot be disposed of. In fact, one of the first experiments where the importance of defect-scattering was detected was based on ARPES.[8] It was shown that the lifetime τ of the Cu(111) surface state actually *decreased* for energies close to E_F, contrary to the predictions of Fermi-liquid theory; this effect was attributed to strong defect-scattering at those energies.

STS, on the other hand, follows the onset of the surface state in the dI/dV signal which is proportional to the density of states, changing shape from steplike (as it would be for a two-dimensional electron system), to obtaining a certain width $\Gamma \sim \tau^{-1}$ due to scattering.[9,10] Additionally, τ can be found via the phase coherence length L_ϕ by probing a quantum interference pattern in the dI/dV curves produced by nanoscale resonators.[11–13] In particular, STS has the advantage that one can choose a defect-free surface region, in order to isolate the electron-electron and electron-phonon scatterings from the defect scattering.[10,14,15]

Whereas in most of the experiments localized defects have been avoided as much as possible, there are a few experimental studies that followed the idea of controlling the defect concentration, in order to extrapolate to a defect-free surface. The first of these experiments has been performed with ARPES for different concentration of potassium atoms on Cu (111),[16] where the structural disorder was investigated and quantified with LEED. In Refs. 17–19, similar experiments have been reported in which the surface-state lifetimes at several coverages of Cu adatoms on Cu (111) have been measured in order to extrapolate to zero-defect concentration.

Theoretical approaches to the surface-state lifetime address, in most cases, the electron-electron and electron-phonon interactions, under the assumption of an ideally defect-free surface. Progress has been made in calculation of the effects of the electron-electron interaction, as the initial degenerate electron gas model[20] was replaced by the more elaborate GW approximation[21] of many-body theory. Applied to image potential states,[22] this approach led to a nice agreement with experiment,[14] accounting for both intraband and interband scattering. Concerning electron-phonon scattering, already

calculations based on the simple Debye model lead to a satisfying agreement between numerical and experimental data,[14] while more accurate *ab initio* calculations of the phonon density of states comprise the investigation of bulk and surface phonons.[23,24] Generally, at low temperatures, the electron-phonon contribution of the scattering rate behaves as $\Gamma = 2\pi\lambda k_B T$ with λ being the electron-phonon coupling parameter. This linear behavior is also found by experiment.[4,6]

However, in particular, on scattering of surface states at adsorbate atoms, only few calculations have been published to date, mainly based on the wave packet propagation method, which is a real-space real-time approach.[25] A systematic theoretical *ab initio* investigation of lifetime reduction caused by (elastic) scattering at different species of adatoms or substitutional impurities in the (111) surfaces of the noble metals is still lacking. Bridging this gap is the purpose of this paper. Furthermore, many of the aforementioned lifetime measurements (especially in STS experiments) have been performed at the lower band edge of the surface-state band, where the contribution to the surface-state linewidth caused by defect scattering merges with the electron-electron and the electron-phonon contribution. This is different at the Fermi energy (at least at low temperatures), where defect scattering becomes the dominant mechanism. In addition, the Fermi level is the relevant energy for transport processes. These are the main reasons, why we have performed our calculations at the Fermi level.

The paper is organized as follows. We start with an introduction to the theoretical formalism, i.e., multiple scattering theory, based on the Korringa-Kohn-Rostoker (KKR) Green function method. We proceed with an analysis of computational and numerical aspects of the calculations, demonstrating differences between full potential calculations and those performed within the atomic sphere approximation. We study the lifetime reduction due to scattering at $3d$ and $4sp$ impurities in the first surface layer and in the fcc adatom position on the noble metal thin films Cu, Ag, and Au, which turn out to show similar trends. While the trend for the scattering rates for impurities in the first surface layer is found to be similar to that calculated in bulk materials[26] (known also from residual resistivity results[27]), the trend for scattering at adatoms remarkably differs. Therefore we focus on adatoms, and analyze the trend of scattering rates for $3d$ and $4sp$ adatoms on Cu(111). This analysis includes an angular-momentum resolved study of surface-state lifetimes as well as a resolution of scattering into bulk and surface states. Finally, the trend observed for magnetic impurities and adatoms is investigated.

A note should be made here on our approximation concerning magnetic impurities. Below the Kondo temperature, the magnetic moment of these defects is quenched by many-body effects.[28] The Kondo temperature varies over orders of magnitude with respect to impurity type and host, depending exponentially on the position of the d resonance and on the hybridization. Therefore there is no "unique" temperature above which all $3d$ impurities become simultaneously magnetic. At a sufficiently low temperature, however, they should all be nonmagnetic in the sense of the Kondo effect. In this case, the nonmagnetic density of states in the local-density approximation does not represent the physical density of states, except exactly at the Fermi energy E_F, where it is probably a good approximation.

This follows from considerations on the Anderson impurity model. In the case of a single localized impurity orbital, the exact solution gives the same phase shift and density of states at E_F as the restricted mean-field solution (i.e., the mean-field solution where the two spin populations are constrained to be equal to each other, which is basically equivalent to a nonmagnetic calculation). In a more general case, the Friedel sum rule reads

$$\Delta Z = -\frac{1}{\pi} \sum_{lm\sigma} \delta_{lm\sigma}(E_F), \qquad (2)$$

where ΔZ is the valence difference between impurity and host while $\delta_{lm\sigma}(E_F)$ is the phase shift at E_F for angular momentum lm and spin σ and is directly related to the scattering matrix and scattering rate. If one assumes that only the d electrons screen the impurity charge of a transition-metal impurity and that all d orbitals are equivalent and have the same phase shift $\delta_d(E_F)$, and additionally takes into account that $\delta_d(E_F)$ is spin independent in the Kondo regime, then the Friedel sum rule reads $\Delta Z = -(10/\pi)\delta_d(E_F)$. Thus the phase shift at E_F is fixed to the same value whether one considers the restricted-mean-field or the exact solution. In reality, the assumption that only the d electrons screen the impurity is an approximation, as is the assumption that the phase shift of all d states is equivalent, since there is a small crystal-field spitting. In practice, however, the two assumptions are relatively well fulfilled, as one can see from comparison of experiment with calculations on the residual resistivity of simple-metal dilute alloys with $3d$ impurities, where the impurity electronic structure was calculated within the density-functional theory and restricted to be nonmagnetic (see, e.g., Refs. 27 and 29). Therefore the results obtained here by the nonmagnetic calculations should be considered to be a reasonable approximation, since only Fermi-level phase shifts enter the calculation. The approximation clearly breaks down for properties that probe the phase shift off the Fermi level, e.g., in the thermopower where the derivative $d\delta_l(E)/dE$ at E_F enters. In this case the density-functional calculations[30] cannot account for the giant thermopower encountered for the Kondo impurities Mn and Fe in Al.

II. THEORY

Details of the KKR method for electronic structure calculations and impurity scattering have been published elsewhere.[31–33] Here we focus on the definition of some quantities that will be useful in the discussion.

In the KKR method, the Bloch wave function $\psi_{\vec{k}}(\vec{r} + \vec{R}^n)$ at a point $\vec{r}$ within an atomic cell n sited at $\vec{R}^n$ is expanded as

$$\psi_{\vec{k}}(\vec{r} + \vec{R}^n; E) = \sum_L c_{\vec{k}nL}(E) R_{nL}(\vec{r}; E), \qquad (3)$$

where the $R_{nL}(\vec{r}; E)$ are regular scattering solutions of the Schrödinger equation of the atom n embedded in free space with boundary condition of an incoming spherical wave of angular momentum $L = (l,m)$, while E denotes the energy eigenvalue. The coefficients $c_{\vec{k}nL}(E)$ are found by the solution of the KKR secular equation for lattice site 0 and propagated by a Bloch factor to any other site.

In the presence of an impurity, an incoming Bloch wave $\psi_{\vec{k}}$ evolves after scattering into an outgoing wave function $\psi_{\vec{k}}^{\text{imp}}$ (with $\vec{k}$ here denoting the initial incoming state). The associated transition amplitude (T matrix),

$$T_{\vec{k}\vec{k}'}(E) := \int d^3r \ \psi_{\vec{k}'}^{\star}(\vec{r}; E) \Delta V(\vec{r}) \psi_{\vec{k}}^{\text{imp}}(\vec{r}; E), \quad (4)$$

is calculated using the expression

$$T_{\vec{k}\vec{k}'}(E) = \sum_{nn'} \sum_{LL'} c_{\vec{k}nL}^{\star}(E) T_{LL'}^{nn'}(E) c_{\vec{k}'n'L'}(E), \quad (5)$$

where the algebraic form of the T matrix

$$T_{LL'}^{nn'} := \sum_{L''} \Delta_{LL''}^{n} \left(\delta_{L''L'}\delta_{nn'} + \sum_{L'''} G_{L''L'''}^{\text{imp},nn'} \Delta t_{L'''L'}^{n'} \right) \quad (6)$$

contains information on the impurity structural Green function $G_{LL'}^{\text{imp},nn'}(E)$ and on the difference in the atomic scattering properties between the embedded impurity and substituted-host atom at site n:

$$\Delta t_{LL'}^{n}(E) := \int_{\text{cell } n} d^3r \ R_{nL}(\vec{r}; E) \Delta V_n(\vec{r}) R_{nL'}^{\text{imp}}(\vec{r}; E), \quad (7)$$

$$\Delta_{LL'}^{n}(E) := \int_{\text{cell } n} d^3r \ R_{nL}^{\star}(\vec{r}; E) \Delta V_n(\vec{r}) R_{nL'}^{\text{imp}}(\vec{r}; E), \quad (8)$$

with $R_{nL'}^{\text{imp}}(\vec{r}; E)$ being the regular scattering solutions of the impurity atom in free space in analogy to the host-atom solutions $R_{nL}(\vec{r}; E)$ [the right-hand side of Eqs. (7) and (8) differ only by the complex conjugation of $R_{nL}(\vec{r}; E)$]. Since $\Delta t_{LL'}^{n}(E)$ and $\Delta_{LL'}^{n}(E)$ vanish at sites where the perturbation of the potential $\Delta V_n(\vec{r})$ is zero, the summation in Eq. (6) is limited to the sites for which the self-consistent potential is appreciably affected by the presence of the impurity; usually the impurity site and its nearest neighbors are sufficient. Only these sites are taken into account also for the calculation of the impurity structural Green function via an algebraic Dyson equation:

$$\begin{aligned} G_{LL'}^{\text{imp},nn'} &= G_{LL'}^{\text{host},nn'} \\ &+ \sum_{n''L''L'''} G_{LL''}^{\text{host},nn''} \Delta t_{L''L'''}^{n''} G_{L'''L'}^{\text{imp},n''n'} \end{aligned} \quad (9)$$

from the host Green function

$$G_{LL'}^{\text{host},nn'}(E) = \frac{1}{\Omega} \int d^2k \, G_{LL'}^{\text{host},\mu\mu'}(\vec{k}; E) e^{i\vec{k}(\vec{R}_{\nu'} - \vec{R}_{\nu})}, \quad (10)$$

where V_{BZ} is the Brillouin zone volume, ν and ν' indicate in-plane lattice vectors, while μ and μ' are layer indices [the site index n is then a combination $n = (\mu, \nu)$] and the energy E can be complex-valued by virtue of the analyticity of the Green function. In practice, to obtain $G_{LL'}^{\text{imp},nn'}$ at E_{F}, we use a small imaginary part of the energy at $E_{\text{F}} + i\epsilon$, where the integral (10) converges; we repeat at $E_{\text{F}} \pm \epsilon + i\epsilon$ so that the derivative of the (analytical) Green function, $dG_{LL'}^{\text{imp},nn'}/dE$ can be found numerically, and we extrapolate the result to the real energy axis by a Taylor expansion, $G_{LL'}^{\text{imp},nn'}(E_{\text{F}}) = G_{LL'}^{\text{imp},nn'}(E_{\text{F}} + i\epsilon) - i\epsilon \, dG_{LL'}^{\text{imp},nn'}/dE$. We use typically $\epsilon = 2$ mRy.

Finally, the probability for an electron scattering from a state $\vec{k}$ to a state $\vec{k}'$ is given by

$$P_{\vec{k}\vec{k}'} = \frac{2\pi}{\hbar} Nc |T_{\vec{k}\vec{k}'}|^2 \delta(E_{\vec{k}} - E_{\vec{k}'}), \quad (11)$$

where N is the total number of atoms in the crystal and c is the impurity concentration (Nc is the number of randomly positioned impurities). Assuming that each impurity scatters independently, the lifetime of a state $\vec{k}$ can be found by summing up the probabilities for scattering of a state $\vec{k}$ into all possible final states $\vec{k}'$:

$$\tau_{\vec{k}}^{-1} = \sum_{\vec{k}'} P_{\vec{k}\vec{k}'} = \frac{2\pi}{\hbar} Nc \sum_{\vec{k}'} |T_{\vec{k}\vec{k}'}|^2 \delta(E_{\vec{k}} - E_{\vec{k}'}). \quad (12)$$

The summation over $\vec{k}'$ can be transformed to an integral, such that the inverse lifetime is obtained by integration over the Fermi surface $S(E_{\text{F}})$:

$$\tau_{\vec{k}}^{-1} = \frac{1}{V_{\text{BZ}}} \frac{2\pi N^2 c}{\hbar^2} \int_{S(E_{\text{F}})} \frac{dS_{\vec{k}'}}{v_{\vec{k}'}} |T_{\vec{k}\vec{k}'}|^2, \quad (13)$$

where $dS_{\vec{k}'}$ is the Fermi surface element and $v_{\vec{k}}$ is the Fermi velocity.

III. COMPUTATIONAL AND NUMERICAL ASPECTS OF THE CALCULATIONS

The electronic structure of the investigated finite-thickness films and defects has been calculated self-consistently within density-functional theory using the principal layer technique implemented in the KKR Green function method[34,35] using the experimental lattice parameter and an angular momentum cutoff of $l_{\text{max}} = 3$. Exchange and correlation effects were included within the local-density approximation to density-functional theory in the parametrization of Vosko *et al.*,[36] while relativistic effects were taken into account in the scalar relativistic approximation (ignoring spin-orbit coupling). Except from Sec. III C, where the difference between full potential (FP) calculations and those performed in the atomic sphere approximation (ASA) is compared, the ASA was used. The perturbed region, where charge relaxation is allowed, is restricted in our calculations to a cluster of 13 sites, thus the shell of nearest neighbors, unless otherwise stated. Structural relaxations are not taken into account, as they could have a quantitative but not qualitative effect to the trends that are related, as we find, to symmetry reduction, reduced screening of adatoms, and the variation of localization of the surface states as a function of film thickness.

Our calculations are performed on finite-thickness films. The situation of a half-infinite crystal with a single surface is approximated by increasing the film thickness up to 40 layers. Furthermore, the vacuum region is described by empty atomic sites at three (or in the FP calculations, four) layers above the surface; these are called "vacuum layers," composed of "vacuum sites."

A. Fermi surfaces of copper, silver, and gold (111) films

The three investigated materials: copper, silver, and gold, crystallize in the fcc structure, have a very similar electronic
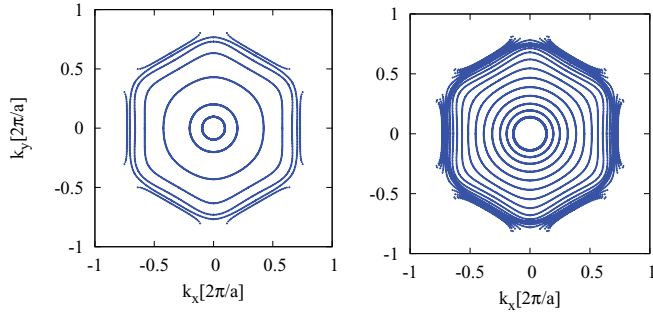
FIG. 1. (Color online) Fermi surfaces of Cu(111) films direction for 6 (left) and 18 layers (right) shown within the first Brillouin zone. In the calculations, three "vacuum layers" have been added on each side. The splitting of the two surface states (represented by the two innermost rings) decreases with the number of layers such that it is not visible in this scale for the 18-layer film (the two innermost rings fall practically on top of each other and appear as a thicker circle).
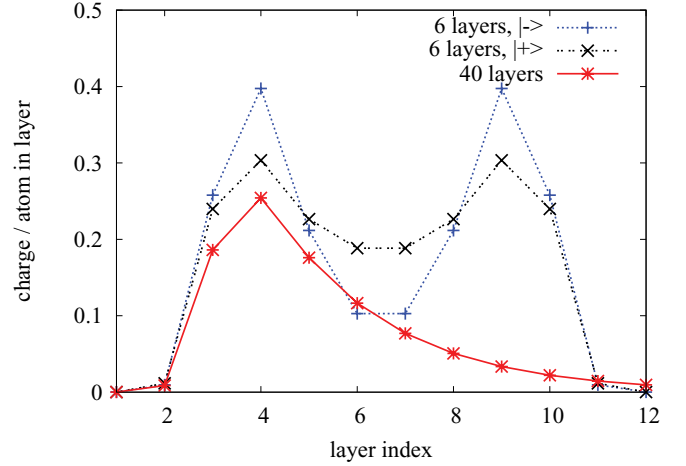

FIG. 2. (Color online) Charge (in units of the electron charge) per atom in the different layers for the two surface states of a copper film with six layers and for the innermost Fermi ring of a copper film with 40 layers (the three outmost layers correspond to vacuum). Here, $|+\rangle$ and $|-\rangle$ denote the bonding and antibonding surface state, i.e., corresponding to the innermost/second innermost Fermi ring, respectively. For the thinner film, the charge in each layer is larger than for the 40-layer film, because the number of layers in which the surface states can penetrate is limited. The two states of the 40-layer film are almost degenerate and nearly indistinguishable in their charge-per-layer picture.

structure and therefore their Fermi surfaces are very similar to each other, too. As these systems are characterized by a two-dimensional periodicity, their Fermi surface consists of one-dimensional curves that form ringlike structures, except in the vicinity of the Brillouin-zone boundary, where hexagonal-like structures occur. The number of rings on the Fermi surface scales linearly with the number of layers, as can be seen in Fig. 1 for the example of a copper (111) Fermi surface for films with six (left) and 18 copper layers (right). The two innermost rings represent the surface bands, which are formed in the gap of the surface-projected band structure.[37] The remaining rings represent bulklike states that should become dense forming a continuum in the limit of infinite thickness. The number of these rings N_B will enter our analysis in Sec. IV B of the trends with respect to film thickness. This analysis in the small-thickness case has a physical meaning only if compared with experiments on free-standing small-thickness films (a situation that is admittedly difficult to achieve) or by approximation on small-thickness films epitaxially grown on insulators.

Surface states are localized at the atomic layers close to the surface and decay exponentially into the bulk and into the vacuum. Since in a finite film there are two surfaces (say "Left" and "Right"), also two surface states ψ_L and ψ_R appear and interact, forming a bonding and an antibonding hybrid, $\psi_\pm = (\psi_L \pm \psi_R)/\sqrt{2}$ with energies $E_\pm(\vec{k})$ (see Fig. 2). The coupling of these two states manifests in a splitting between the two inner rings of the Fermi surfaces, decreasing with increasing film thickness since the overlap of the two surface states decreases exponentially. In the sections on the lifetime calculation, we show results on the innermost surface-state ring at $k_x > 0$, $k_y = 0$, noting that the lifetime $\tau_{\vec{k}}$ changes only very weakly for different $\vec{k}$ corresponding to the same surface-state ring due to the isotropic character of the surface states.

For small film thicknesses (less than 10–15 layers), we retain the term "surface states" for $\psi_\pm$ in our analysis in Secs. IV B and V, although in reality, their amplitude has not yet fully decayed in the middle of the film, so that they are rather like quantum-well states. In the limit of infinite film thickness only one of the two surface bands survives at each surface (either ψ_L or ψ_R). However, the overlap of

these states with the surface impurity is higher by a factor $\sqrt{2}$ compared to the overlap of $\psi_\pm$ with the impurity. Therefore, for comparison with experiments performed not on ultrathin films but on crystal surfaces, the scattering rates, which are calculated here in the $\psi_\pm$ basis (more precisely, involving the ψ_+ as an initial state), can be taken from the thick but finite film calculations but have to be multiplied by a factor of 2.

B. Testing of the lifetimes via the optical theorem

Contrary to the case of bulk systems where momentum-relaxation times and residual resistivities due to scattering at impurities have been calculated in *ab initio* calculations (e.g., in Refs. 26,27, and 38), there are no numerical or experimental references to compare our results of lifetime reduction of surface states caused by adatom scattering. However, another possibility to attest the numerical correctness of the results is given by the optical theorem, according to which the elements of the scattering matrix $T_{\vec{k}\vec{k}'}$ must obey

$$-\frac{2Nc}{\hbar}\mathrm{Im}T_{\vec{k}\vec{k}} = \frac{2\pi N^2 c}{V_{BZ}\hbar} \int_{S(E_{\vec{k}})} \frac{dS_{\vec{k}'}}{\hbar v_{\vec{k}'}} |T_{\vec{k}\vec{k}'}|^2 \equiv \tau_{\vec{k}}^{-1}. \quad (14)$$

This identity turns out to be a very sensitive consistency probe. Also, it is numerically fulfilled only if the numerical convergence of the quantities involved is very good. We have calculated surface-state scattering rates $\tau_{\vec{k}}^{-1}$ for impurities in the first surface layer as well as in adatom position on top of the surface at the fcc threefold hollow site on a six layers Cu(111) film via both sides of Eq. (14). The deviation between the left and the right sides of Eq. (14) was in all cases less than 1.5% (the latter deviation was obtained for surface-state scattering rates off impurities in adatom position in FP calculations). The
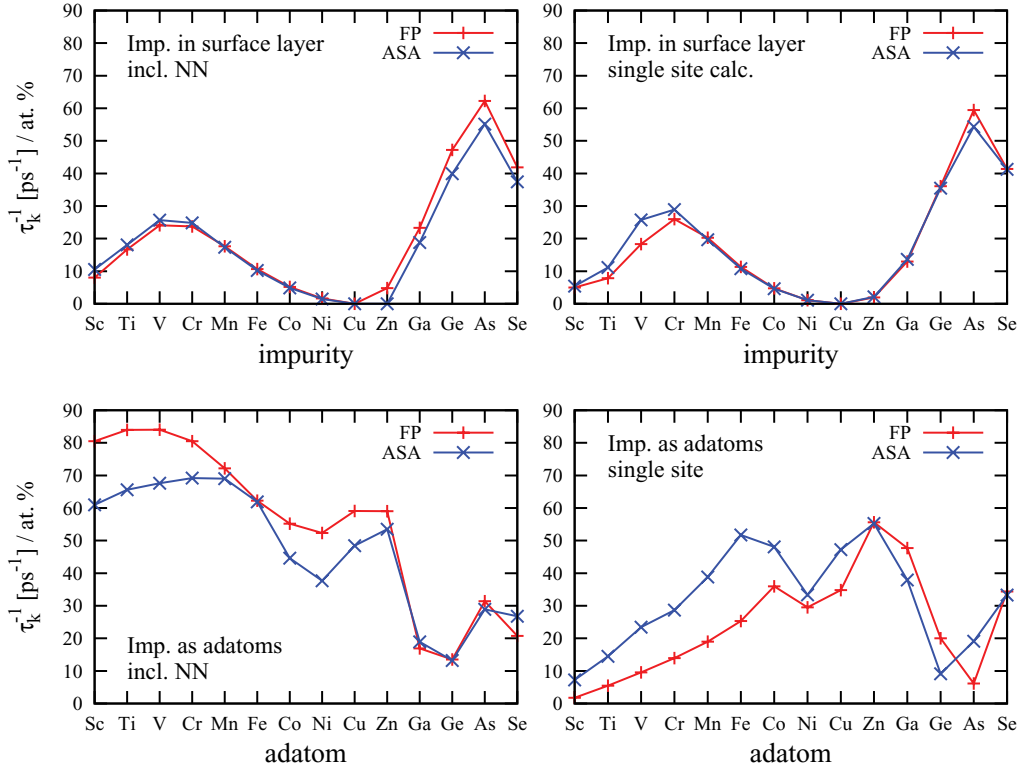
FIG. 3. (Color online) Scattering rates $\tau_{\vec{k}}^{-1}$ for impurities in the first surface layer (upper panels) and adatoms (lower panels) obtained within the atomic sphere approximation and full-potential calculations. While the agreement between the two calculations is very good for impurities in the first surface layer, for adatoms, the two calculation schemes lead to qualitatively similar but quantitatively different results. On the left, results of multiple-site calculations are shown, i.e., with a cluster of the nearest neighbors included in the potential perturbation. On the right, the comparison is shown for single-site calculations.

accuracy of the calculations is very sensitive to the number of $\vec{k}$ points used for the calculation of the structural Green function of the host in Eq. (10), $G_{LL'}^{\text{host},nn'}(E)$, which is used to calculate the impurity Green function $G_{LL'}^{\text{imp},nn'}(E)$ via the Dyson equation (9). We typically use a $\vec{k}$ mesh of 500×500 in the two-dimensional Brillouin zone for the calculation of the scattering properties satisfying the optical-theorem test, while a mesh of 40×40 is already enough for the self-consistent potential. Additionally, four vacuum layers are necessary to obtain the above mentioned accuracy, so that the surface and impurity states at E_F vanish at the outmost vacuum layer.

C. Comparison of ASA versus FP and single-site versus multiple-site calculations

The computational effort in ASA is lower than in FP calculations. However, at surfaces, where the symmetry is broken, nonspherical components of the potential could play an important role. Therefore, for the example of a film of six layers of copper, surface-state lifetimes within ASA and FP calculations are calculated and compared to each other.

The results are presented in Fig. 3. In the two panels on the left, the self-consistent perturbed potential of the impurity and the nearest neighbors (13 sites in total, which we call a *multiple-site* calculation) has been included in the calculation of the scattering matrix $T_{\vec{k}\vec{k}'}$. In the two panels on the right, calculations in the *single-site-approximation* are presented, i.e., only the impurity site is taken in the summation of Eq. (5),

but with the impurity potential previously converged using also the nearest-neighbors perturbation. All scattering rates, i.e., inverse lifetimes $\tau_{\vec{k}}^{-1}$, are given in units of ps^{-1} per atomic percent of impurities.

For impurities in the first surface layer (the results are shown in the two upper panels of Fig. 3), the agreement between the ASA and FP schemes is very good, both for single-site and multiple-site calculations. This is not the case for adatoms as can be observed in the two lower panels of the same figure where a quantitative difference of maximal 25% can be observed. Nevertheless, the trends in FP and ASA are qualitatively similar. Since we are interested in these trends, we will restrict our further calculations to the ASA.

The qualitative difference between single-site multiple-site calculations in the case of adatoms raises the question whether the cluster consisting of nearest neighbors is large enough to obtain converged results. Therefore multiple-site calculations (not shown here) including additionally the shells up to the third nearest neighboring sites (43 atoms in total) have been performed. They show that the results remain practically stable beyond the nearest-neighbor approximation, which we adopt henceforth.

IV. ANALYSIS OF SURFACE-STATE LIFETIMES OF Cu FILMS

The most striking feature of our results is the qualitative difference between the trends of scattering rates at adatoms
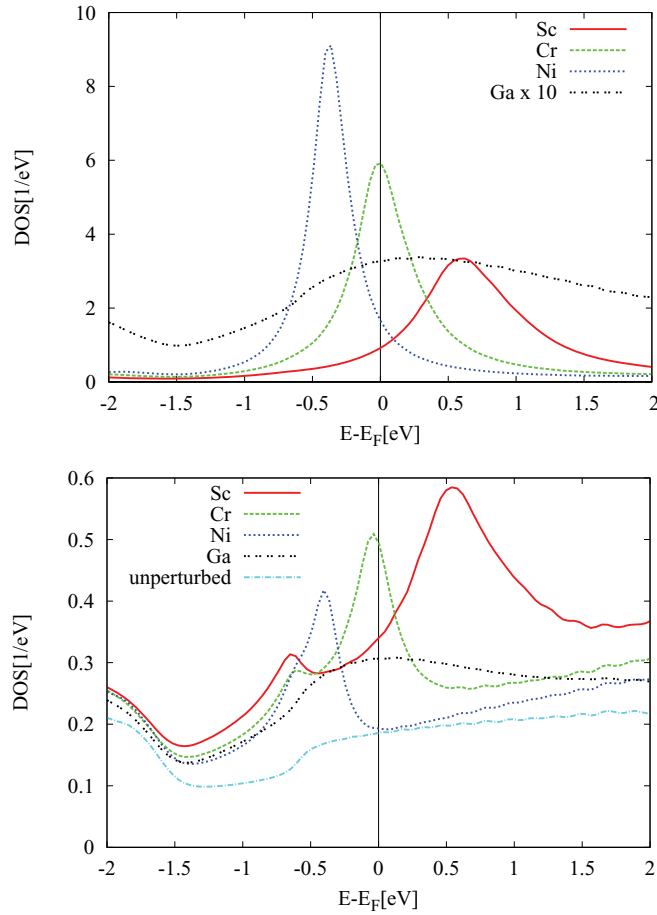
FIG. 4. (Color online) (Top) Local density of states of Sc, Cr, Ni, and Ga adatoms on a Cu(111) film of 40 layers. The density of states does not differ qualitatively from that of impurities in the surface layer. (Bottom) Density of states summed over the vacuum sites surrounding the adatoms.

and those of impurities in the surface, as can be seen in Fig. 3. While the trend for impurities in the first surface layer (upper panel) resembles that which has been found for scattering at impurities in bulk,[26,27] the trend for the scattering rate at adatoms (lower panel) does not.

In the case of impurities in the first surface layer as well as in bulk, the observed trend follows the local density of states of the impurities (see Fig. 4): For the d scatterers, the scattering rate shows a peak with a maximum at V and Cr as the d resonance crosses the Fermi energy. Then, as the p states start crossing E_F, the scattering rate increases again starting off quadratically with respect to the difference in valency between impurity and host according to Linde's rule.[39,40]

Basically, this correlation between the impurity local density of states and the scattering strength of impurities can be traced back to conditions which are not necessarily met for adatoms. The first condition is that the screening of the impurity charge in metals takes place mostly in the impurity atomic cell. Thus the perturbation of the potential in nearby cells is rather small, while the impurity wave functions are relatively atomic-like in the cell and matched to phase-shifted host waves outside. The second condition is that the free-electron-like behavior in the bulk of normal metals

together with the nearly spherical symmetry of the impurity potential allows for independent scattering of the s, p, and d without mutual interference. Thus the angular-momentum resolved local density of states reflects the scattering properties of the angular-momentum channels independently to each other.

For adatoms, however, the screening is not as efficient, thus the atomic size can increase significantly. Here, by atomic size, we mean the volume in which the impurity induces a significant potential perturbation. In addition, the reduced symmetry allows for interference between different angular momenta, notably (as we will see) between s and p_z. Impurities in the surface layer are apparently close enough to the impurity-in-bulk situation that they behave in the same way.

Having in mind these comments, we proceed to an analysis of the results.

A. Adatom scattering

Considering the trend of adatom-scattering rates in the multiple-site approach (see the left-bottom panel of Fig. 3), there are two features to observe. The first part of the trend (from Sc to Fe/Co) is dominated by a relatively large scattering rate, showing a plateau which is absent in the single-site calculations (right-bottom panel of Fig. 3). On the other hand, the second part of the curve (from Ni to Se) is qualitatively the same for single-site and multiple-site calculations. However, it behaves in an uncommon manner, showing a kinklike structure, which is completely different from the trend for the sp impurities in the surface.

The plateau in the scattering rates of the early $3d$ scatterers can be understood by the significant difference between the single-site approximation compared to multiple-site calculations (see Fig. 5), which hints at an atomic size effect. These atoms (Sc, Ti, V) have relatively large atomic radii (which are $r_{at} = 1.62$ Å for Sc, 1.45 Å for Ti, 1.34 Å for V)[41] and therefore extend much more into the vacuum than e.g. a Ni adatom with $r_{at} = 1.24$ Å. This is not any more the case for atoms embedded in the surface or in bulk, as the strong screening strongly reduces the atom size. In order to verify this line of arguments, we have performed additional calculations where—apart from the adatom site—only the perturbed surrounding vacuum sites or only the perturbed substrate Cu atoms are included in the expression for $T_{\vec{k}\vec{k}'}$ [see the summation over sites n and n' in Eq. (5)]. These calculations reveal that the largest contribution next to the adatom site arises from the surrounding vacuum potential and *not* from the Cu atoms in the surface layer. We also examined the density of states at E_F around the impurity, shown in the lower panel of Fig. 4. We found that, indeed, there is an increased DOS in the vacuum around the early $3d$ adatoms, while this contribution is reduced for the late $3d$ series. When the p states start crossing E_F (at Ga) the size of the atom grows again, but apparently the qualitative trend is governed by different effects (see next paragraph), although there are some quantitative differences between single- and multiple-site calculations. The larger extent of the early $3d$ adatoms also manifests in a larger charge transfer to the surrounding vacuum sites. This becomes visible in the lower panel of Fig. 5, where we show the charge ΔQ in the surrounding vacuum sites induced by the adatom.
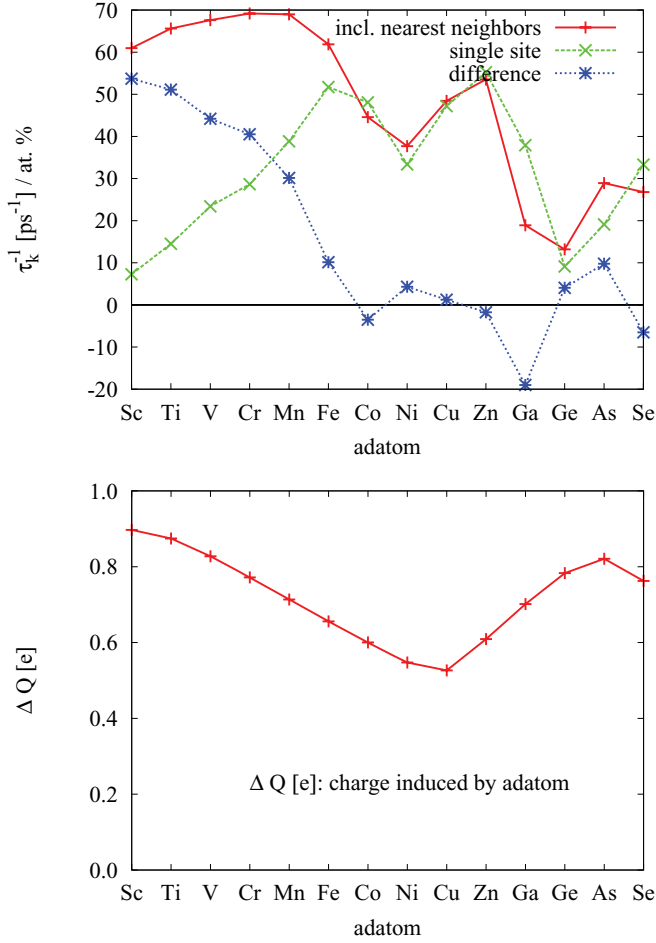
FIG. 6. (Color online) Angular-momentum resolved scattering rates for adatoms on a 40-layer Cu(111) film. The inclusion of just the s and the p_z channel in the single-site scattering matrix $T_{LL'}^{00}$ [compare Eq. (6)] for the $4sp$ adatoms is already a good approximation for the total scattering rate. Scattering in only the s channel by far overestimates the total scattering rate. The same can be observed for Ge, As, and Se adatoms when scattering is restricted to the p channel. The total scattering rate is then reduced due to a destructive interference of s and p scatterings, which can be verified by the investigation of Friedel oscillations (see Fig. 7).

FIG. 5. (Color online) (Top:) Surface-state scattering rate $\tau_{\vec{k}}^{-1}$ in ps^{-1} per atomic percent for scattering at adatoms. Red curve: multiple-site calculations. Green curve: single-site approximation. Blue curve: difference between the two cases. (Bottom) Excess charge (in electron-charge units) induced by adatoms in the surrounding vacuum sites. For the d adatoms, the trend observed in the difference between the scattering rates calculated including nearest neighbors and single-site scattering is similar to the trend of the charge induced by the adatoms.

In order to understand the second part of the trend for scattering at adatoms (from Ni up to Se), which shows a zigzag structure, we analyze the single-site results, because qualitatively they do not differ from multiple-site results, while they allow for an angular-momentum resolved investigation of scattering rates. Thus we restrict the single-site contribution $n = n' = 0$ of the scattering matrix $T_{LL'}^{nn'}$ defined in Eq. (6) to different L channels. The results are presented in Fig. 6 for T_{ss}^{00} and T_{pp}^{00} together with the total single-site contribution. A restriction of scattering to only the s or only the p channel significantly overestimates the result for many adatoms. The conclusion is that there is destructive interference between the s and the p_z channels that is allowed by the breaking of symmetry due to the surface. The zigzag structure, with a peak at Zn and a dip at Ge, occurs because the maxima of the s and p channels are phase shifted with respect to each other.

For a more elaborate analysis of interference effects we have calculated Friedel oscillations, confining again the
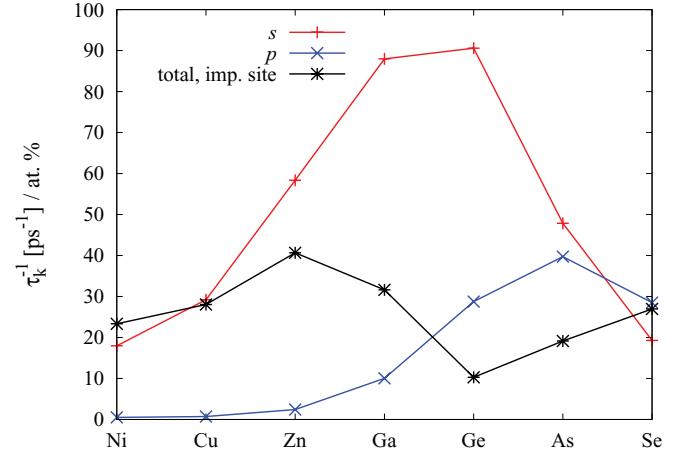
scattering to particular L channels. We obtain the change in the site-integrated density of states, $\Delta n_L(E_{\mathrm{F}}; R) = n_L^{\mathrm{imp}}(E_{\mathrm{F}}; R) - n^{\mathrm{host}}(E_{\mathrm{F}}; R)$, where L indicates the allowed scattering channel and R is the lateral distance from the adatom in the first vacuum layer. In this way, we are able to see, in real space, the relative phase shift in channels that are expected to interfere, e.g., between the s and p_z channels. This analysis is presented in Fig. 7 as a function of the distance from the adatom site. We see that oscillations in the s and p_z channels are mutually phase shifted and interfere destructively.

B. Separation of scattering into bulk and surface states

After a scattering event, an electron that was previously occupying a surface state $\vec{k}_{\mathrm{surf}}$ can end up in another surface state $\vec{k}'_{\mathrm{surf}}$ or in a bulk state $\vec{k}'_{\mathrm{bulk}}$. The distinction between the two cases can be of importance to effects such as surface-state mediated interactions between defects, surface resistivity, the lifetime of surface plasmons, etc. The method used to calculate the surface-state lifetimes given in Sec. II, Eq. (13), allows to distinguish between the two cases. The total scattering rate of a (surface) state characterized by a wave vector $\vec{k}$ is composed of a contribution $1/\tau_{\vec{k}}^{\mathrm{surf}}$ given by

$$\frac{1}{\tau_{\vec{k}}^{\mathrm{surf}}} = \frac{2\pi N^2 c}{V_{\mathrm{BZ}} \hbar^2} \int_{S(E_{\mathrm{F}})_{\mathrm{surf}}} \frac{dS_{\vec{k}'}}{v_{\vec{k}'}} |T_{\vec{k}\vec{k}'}|^2, \qquad (15)$$

where the integration is performed only over the surface bands and analogously a contribution $1/\tau_{\vec{k}}^{\mathrm{bulk}}$, where only the bulk end states of the Fermi surface are taken into account:

$$\frac{1}{\tau_{\vec{k}}^{\mathrm{bulk}}} = \frac{2\pi N^2 c}{V_{\mathrm{BZ}} \hbar^2} \int_{S(E_{\mathrm{F}})_{\mathrm{bulk}}} \frac{dS_{\vec{k}'}}{v_{\vec{k}'}} |T_{\vec{k}\vec{k}'}|^2. \qquad (16)$$
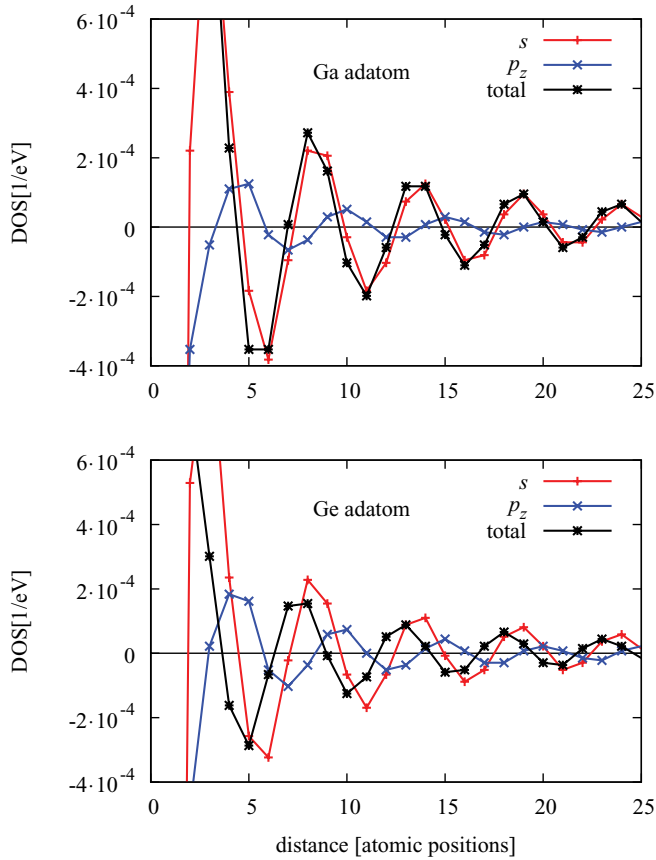
FIG. 7. (Color online) Friedel oscillations in the vacuum near the surface and as a function of the distance from the impurity calculated for Ga and Ge adatoms on Cu. The difference of the local density of states as a function of distance to the adatom site is calculated, i.e., $n_L^{\text{imp}}(E_{\text{F}}; R) - n^{\text{host}}(E_{\text{F}}; R)$, with $n^{\text{host}}(E_{\text{F}}; R)$ the density of states of the vacuum site of the host and $n_L^{\text{imp}}(E_{\text{F}}; R)$ the density of states of the same site perturbed by the adatom. Here, the index L means that the scattering has been artificially confined to the L channel only (s or p_z). Both for Ga and Ge adatoms, a destructive interference of the s and p_z channels is observed as they are out of phase. d scattering is found to be very small and can be neglected.

Obviously, considering the definitions of $\tau_{\vec{k}}$, $\tau_{\vec{k}}^{\text{surf}}$, and $\tau_{\vec{k}}^{\text{bulk}}$, the relation

$$\frac{1}{\tau_{\vec{k}}} = \frac{1}{\tau_{\vec{k}}^{\text{surf}}} + \frac{1}{\tau_{\vec{k}}^{\text{bulk}}} \quad (17)$$

holds.

The two contributions have been calculated for films consisting of six and 40 layers of copper for impurities in the surface layer as well as for adatoms and are presented in Fig. 8. The purpose of varying the film thickness was primarily to approach the physics of ultrathin films (in the sense that was discussed in Sec. III A).

The most important observation is that $1/\tau_{\vec{k}}^{\text{bulk}}$ and $1/\tau_{\vec{k}}^{\text{surf}}$ are on the same order of magnitude, even in the case of adatoms. Naturally, variations occur as a function of film thickness, which we will now address.

Qualitatively, we expect that the relative scattering rate into bulk and surface states should depend on (i) the amplitude of the surface states $\psi_S(\vec{R}_{\text{imp}})$ at the impurity site, (ii) the

amplitude of the bulk states, $\psi_B(\vec{R}_{\text{imp}})$ at the impurity site, and (iii) the available number of bulklike states, N_B. About point (i), as a function of the number of layers in the film N_L, $\psi_S(\vec{R}_{\text{imp}})$ first decreases before reaching saturation, since in very thin films the number of layers in which the surface states can penetrate is limited (see also Fig. 2). From this effect alone we expect an overall reduction of both $1/\tau_{\vec{k}}^{\text{surf}} \sim |\langle\psi_S(\vec{R}_{\text{imp}})|T|\psi_S(\vec{R}_{\text{imp}})\rangle|^2 \sim |\psi_S(\vec{R}_{\text{imp}})|^4$ and $1/\tau_{\vec{k}}^{\text{bulk}} \sim |\langle\psi_S(\vec{R}_{\text{imp}})|T|\psi_B(\vec{R}_{\text{imp}})\rangle|^2 \sim |\psi_S(\vec{R}_{\text{imp}})|^2$ with increasing N_L before a saturation takes place, but with $1/\tau_{\vec{k}}^{\text{surf}}$ being more strongly affected due to the 4th power of the amplitude. About point (ii), $\psi_B(\vec{R}_{\text{imp}}) \sim 1/\sqrt{N_L}$, yielding a factor of $1/N_L$ to $1/\tau_{\vec{k}}^{\text{bulk}}$; however, this reduction is partly compensated by point (iii), which contributes a factor $N_B = N_L - 1$ to $1/\tau_{\vec{k}}^{\text{bulk}}$.

Combining (i), (ii), and (iii) gives a behavior of the form $1/\tau_{\vec{k}}^{\text{bulk}} \sim |\psi_S(\vec{R}_{\text{imp}})|^2(1 - 1/N_L)$ for scattering into bulk states, which should show a saturation for large N_L, but could be either increasing or decreasing at small N_L depending on the relative importance of the two terms. On the other hand, point (i) gives a behavior of the form $1/\tau_{\vec{k}}^{\text{surf}} \sim |\psi_S(\vec{R}_{\text{imp}})|^4$ for scattering into surface states, which should be first decreasing with N_L and then also saturating.

The qualitatively expected behavior is consistent with our calculations (see Fig. 8). The scattering rates into surface states are larger for the six-layer film than for the 40-layer film by approximately a factor of 2, while the scattering rates into bulk states are a little larger for the 40-layer film.

V. COMPARISON BETWEEN Cu, Ag, AND Au FILMS

In the previous section, we have analyzed surface-state lifetimes for impurities in and on copper films. Here, we extend our investigations to silver and gold films. Even though the band structure of the three noble metals is similar, differences in the thickness dependence are found mainly due to the change of energetic position of the surface state, especially in Ag.

The calculated data, shown in Fig. 9, are qualitatively similar for all three hosts. Scattering rates off adatoms are largest for the first elements of the row and remain almost constant until Mn; just as in the case of the copper film (see previous section), this should be due to the larger atomic radius entailing a larger extent of these adatoms into the vacuum. Furthermore, all three host materials show a clear trend that scattering at adatoms on a film of six layers is enhanced compared to that of larger thickness. The reason is the higher localization of the surface state for thin films, as explained in the Cu(111) case.

We show here results for the innermost surface state only (in the sense of Sec. III A), whose lifetime, especially for the six-layer films and for some adatoms, remarkably differs from that of the second surface state. While for the early $3d$ elements, the difference is relatively small (a few percent), it can increase up to 60% for Ge and 48% for As adatoms. For the 40-layer film, this difference almost vanishes as does the splitting between the two surface bands.

Concerning scattering at impurities in the surface, the situation is somewhat complicated. Qualitatively, for all three
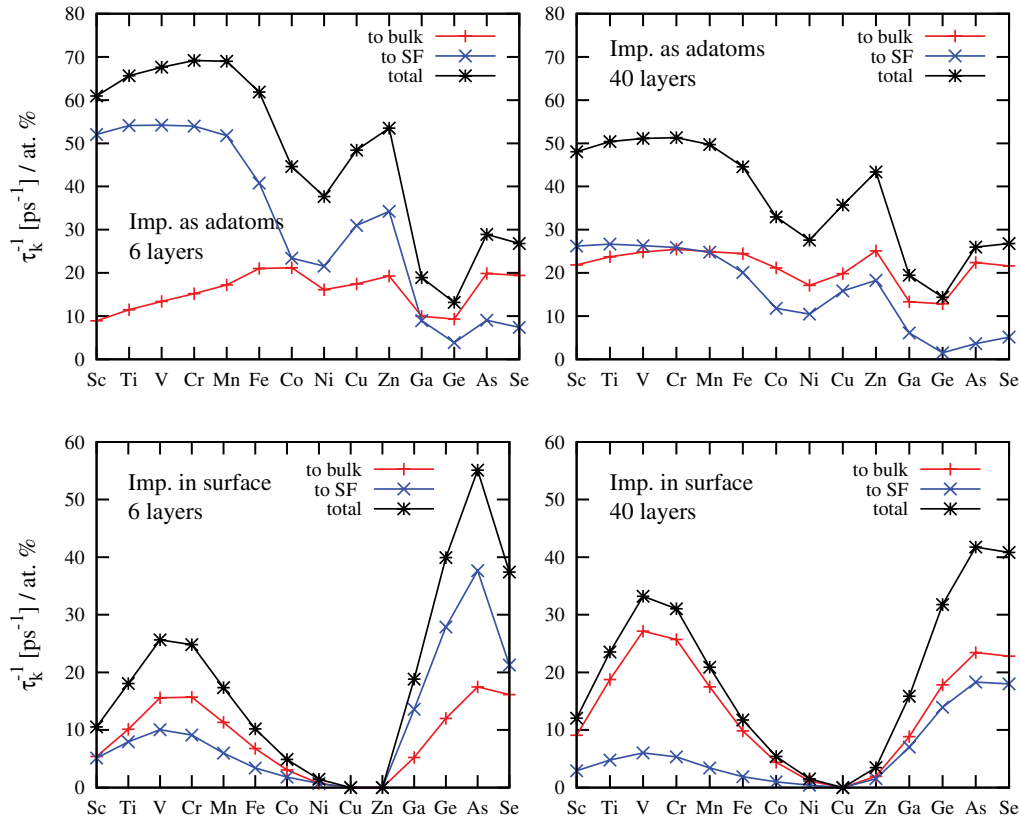
FIG. 8. (Color online) Scattering rate $\tau_{\bar{k}}^{-1}$ for the innermost surface state together with the contributions of scattering rates to bulk and surface states $1/\tau_{\bar{k}}^{\text{bulk}}$ and $1/\tau_{\bar{k}}^{\text{surf}}$ for films with six layers (left) and 40 layers of copper (right) for adatoms (top) and impurities in the first surface layer (bottom).

host materials, a clear maximal scattering rate for the $3d$ elements with half-filled shells (V, Cr) is observed as well as high scattering rates for the sp scatterers. Hence, as expected, the global trend reflects the situation of scattering at impurities in the bulk. However, large quantitative differences among the three host materials are observed when considering the thickness dependence as well as the comparative scattering strength of $3d$ and $4sp$ impurities. While for a copper host, the scattering rate does not depend much on the film thickness, especially for silver films, the thickness can change the scattering rate up to almost an order of magnitude. Actually, such a strong variation in the Ag films is reasonable, because of the relatively shallow position of the surface state with respect to the Fermi energy.[42] As a result, in thin films, quantum-confinement effects push one of the two surface states (the innermost ring) above E_F and the other lower, resulting in a significant change of the available phase space for scattering. In thicker films, the two states are approximately degenerate and below E_F. In any case, in Ag the scattering rate into surface states is small due to the smallness of the corresponding Fermi rings.

Further difference among the scattering rates in the three metals can arise from the localization of the surface states. In the case of impurity scattering, we expect that more localized surface states (penetrating less into the bulk region) should be more susceptible to scattering into bulk states, as the arguments following point (i) in Sec. IV B show, i.e., the

scattering potential is localized at the surface. However, at higher temperatures, the surface states can decay into bulk states due to phonon or many-body effects. Then, surface states that are less localized (penetrating more into the bulk) should scatter more efficiently into bulk states, since the scattering potential (electron-phonon or electron-electron interaction) extends over the whole film. This line of argumentation is suggested in the work Tsirkin *et al.*[43] who analyzed the lifetime of image-states in Ag(111). A higher localization of the surface states of Cu(111) compared to Ag(111) was recently observed and analyzed by Lobo-Checa *et al.*[44] and could be related to the higher scattering rate observed for impurities in the surface of thick Cu films compared to Ag (see Fig. 9, right panels).

A comparison to other theoretical or experimental results is not possible because of lack of data; although these surface states have been subject of many experiments, to our knowledge, no experiments have been performed in which the surface-state lifetimes due to scattering at the specific impurities at the Fermi level have been measured. However, the order of magnitude of the calculated scattering rates should allow for an experimental detection, which, e.g., in ARPES reaches a few milli electron volts. To compare, in inverse photoemission spectroscopy a linewidth of about 23 meV $\approx$ 35ps$^{-1}\hbar$ for Cu, 6 meV $\approx$ 9ps$^{-1}\hbar$ for Ag, and 21 meV $\approx$ 33ps$^{-1}\hbar$ for Au for electron-electron scattering processes has been measured.[5] A measurement for 1% of defects should be, therefore, within the experimental resolution.
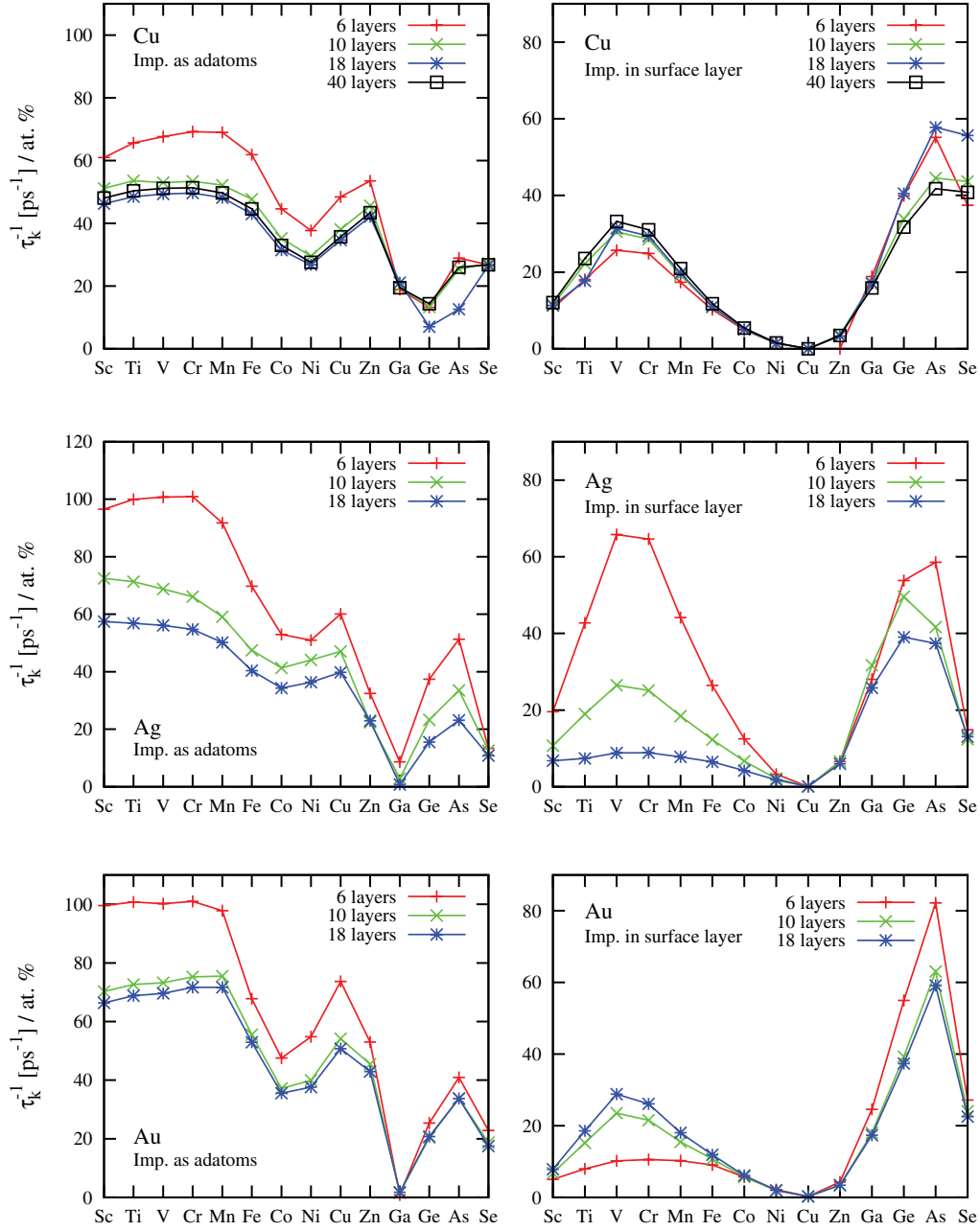
FIG. 9. (Color online) Surface-state scattering rate $\tau_{\vec{k}}^{-1}$ for adatoms (left) and impurities in the first surface layer (right) for Cu, Ag, and Au films with different number of layers. For silver films, the scattering rate is most sensitive to the film thickness due to the fact that one of the surface bands lies above E_F in the six and 10 layer cases. Qualitatively, the trend as a function of the impurity atomic number is similar for the three hosts.

VI. SCATTERING AT MAGNETIC IMPURITIES

So far, only scattering at nonmagnetic impurities and adatoms has been considered, in an approximation that was explained in Introduction. However, above the Kondo temperature, some of the $3d$ impurities become magnetic and scattering in the two spin channels has to be treated separately. We investigate now the consequences of spin polarization, showing results for the Cu(111) surface only, which suffices to demonstrate the main effect of a double-peak structure in the scattering rate.

The calculated lifetimes are shown in Fig. 10 for a 40-layer film. In the adatom position the $3d$ elements starting between Ti and Ni are magnetic, while as impurities in the surface, Ti and Ni are paramagnetic. The $4sp$ elements are in all cases nonmagnetic. The magnetism of the $3d$ elements leads to an expected double-peak structure in the trend of the scattering rates, which is already known, e.g., for residual resistivity in bulk above the Kondo temperature[45–48] and originates from the offset of the d resonances of the two spin channels, which are mutually repelled by the exchange interaction. Thus a first peak
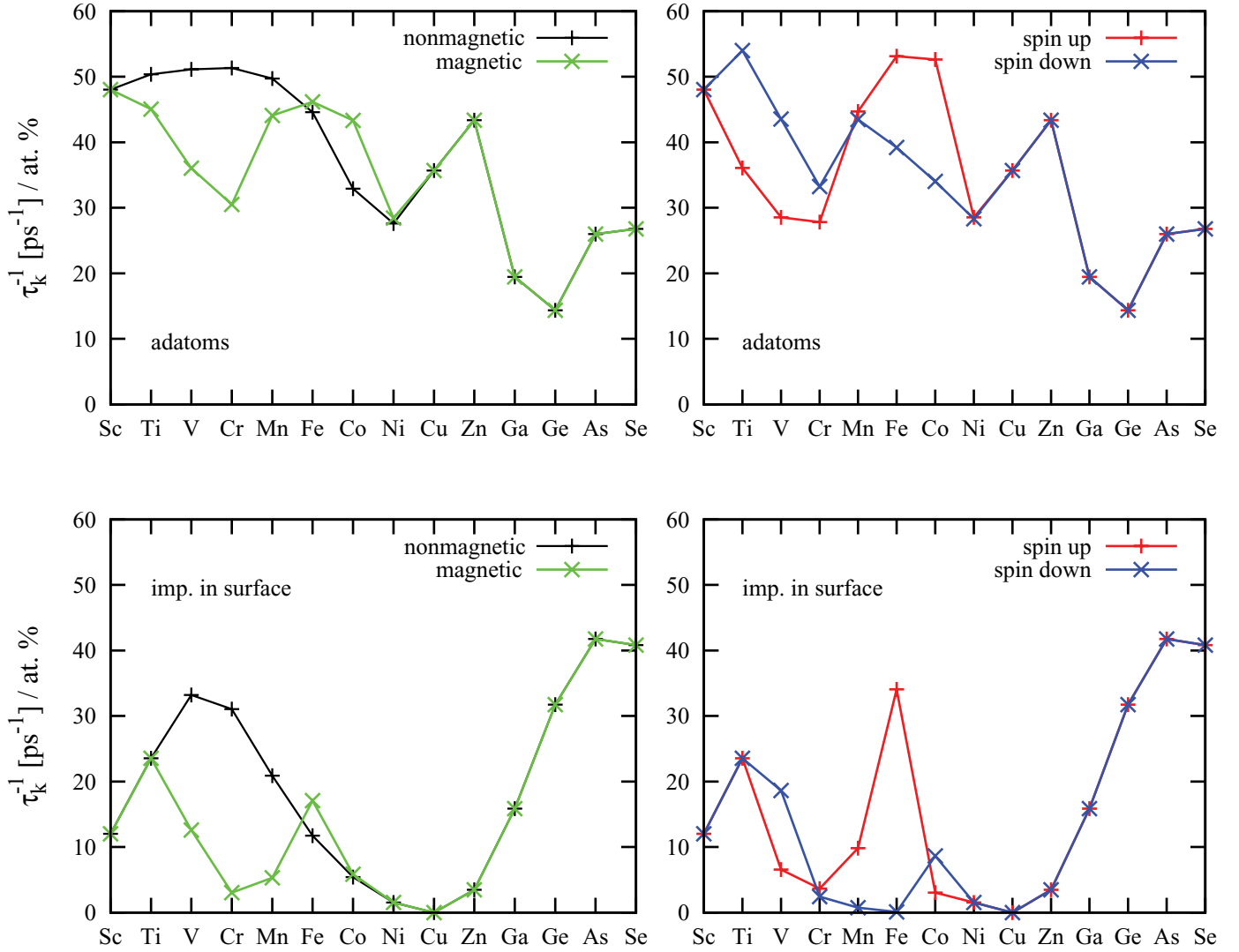
FIG. 10. (Color online) Scattering rate of the surface state at magnetic adatoms (top) and impurities in the surface layer (bottom) of a 40-layer Cu(111) film. The spin polarization of the 3d elements leads to a double-peak structure of $\tau_{\vec{k}}^{-1}$ because of the exchange splitting in the density of states of the two spin channels. The first maximum is reached for Ti, when the d resonance of the spin-up channel crosses the Fermi level, while the second maximum corresponds to the localization of the d resonance of the spin down channel at E_F. On the right, the spin-resolved results are shown.

of the scattering rate is observed for Ti, where the d resonance of the majority channel is centered at the Fermi level, while a second peak appears for Fe and Co in the minority-spin channel. For Cr impurities, where scattering rates are large in the case of paramagnetic impurities, the scattering rate is most drastically reduced as E_F lies between the resonances.

VII. SUMMARY

In summary, we have presented a systematic study of the lifetime of the (111) surface state of the noble metals considering scattering at the Fermi energy due to 3d and 4sp impurities atoms on and in the surface. Our main finding is a qualitatively different trend, as a function of the impurity atomic number, for adatoms compared to surface-embedded impurities. While the latter case is similar to the trend for impurities in the bulk, reflecting the sharpness of the d

resonance and Linde's rule as the d and p states cross the Fermi level, adatom scattering is found to be dominated by other criteria such as the size of the adatom and interference effects between the scattering amplitudes of different angular momenta. The conclusion is that the surface strongly affects the scattering properties by the reduction in charge screening as well as by the lowering of symmetry.

A separation of scattering rates into surface-to-surface and surface-to-bulk parts shows that the two contributions are comparable in magnitude for adatoms as well as for embedded impurities. Additionally, in the case of ultrathin films we have found that the scattering into surface-states contribution decreases with film thickness, since the surface state extends further into the bulk in thicker films, and finally saturates. Furthermore, we have found that the lifetime is sensitive on the film thickness, especially for Ag. This is due to the very shallow surface state of Ag, which can be shifted in

energy due to quantum confinement effects, changing the available phase space for scattering. The calculated lifetimes should be detectable as a surface-state linewidth within the resolution of photoemission spectroscopy already for impurity concentrations 1%.

*Ph.Mavropoulos@fz-juelich.de

[1] J. Kröger, M. Becker, H. Jensen, T. von Hofe, N. Néel, L. Limot, R. Berndt, S. Crampin, E. Pehlke, C. Corriol *et al.*, Prog. Surf. Sci. **82**, 293 (2007).

[2] H. C. Manoharan, C. P. Lutz, and D. M. Eigler, Nature (London) **403**, 512 (2000).

[3] L. Vitali, P. Wahl, M. A. Schneider, K. Kern, V. M. Silkin, E. V. Chulkov, and P. M. Echenique, Surf. Sci. **523**, L47 (2003).

[4] B. A. McDougall, T. Balasubramanian, and E. Jensen, Phys. Rev. B **51**, 13891 (1995).

[5] F. Reinert, G. Nicolay, S. Schmidt, D. Ehm, and S. Hüfner, Phys. Rev. B **63**, 115415 (2001).

[6] F. Reinert, B. Eltner, G. Nicolay, F. Forster, S. Schmidt, and S. Hfner, Physica B **351**, 229 (2004).

[7] J. Kröger, L. Limot, H. Jensen, R. Berndt, S. Crampin, and E. Pehlke, Prog. Surf. Sci. **80**, 26 (2005).

[8] S. D. Kevan, Phys. Rev. Lett. **50**, 526 (1983).

[9] L. Limot, E. Pehlke, J. Kröger, and R. Berndt, Phys. Rev. Lett. **94**, 036805 (2005).

[10] J. Li, W.-D. Schneider, R. Berndt, O. R. Bryant, and S. Crampin, Phys. Rev. Lett. **81**, 4464 (1998).

[11] J. Kliewer, R. Berndt, and S. Crampin, New J. Phys. **3**, 22 (2001).

[12] H. Jensen, J. Kröger, R. Berndt, and S. Crampin, Phys. Rev. B **71**, 155417 (2005).

[13] J. Li, W. D. Schneider, S. Crampin, and R. Berndt, Surf. Sci. **422**, 95 (1999).

[14] J. Kliewer, R. Berndt, E. V. Chulkov, V. M. Silkin, P. M. Echenique, and S. Crampin, Science **288**, 1399 (2000).

[15] The temperature dependence of the contribution of the electron-phonon coupling to the surface-state linewidth can be addressed by ARPES only, since at elevated temperature STS measurements do not lead to significant results: this is due to a change of the width of the Fermi distribution function[49] and thus an intrinsic broadening.

[16] S. D. Kevan, Phys. Rev. B **33**, 4364 (1986).

[17] F. Theilmann, R. Matzdorf, G. Meister, and A. Goldmann, Phys. Rev. B **56**, 3632 (1997).

[18] F. Theilmann, R. Matzdorf, and A. Goldmann, Surf. Sci. **420**, 33 (1999).

[19] T. Fauster, C. Reuß, I. L. Shumay, M. Weinelt, F. Theilmann, and A. Goldmann, Phys. Rev. B **61**, 16168 (2000).

[20] J. J. Quinn, Phys. Rev. **126**, 1453 (1962).

[21] L. Hedin and S. Lundqvist, *Solid State Physics: Advances in Research and Applications*, edited by F. Seitz, D. Turnbull, and H. Ehrenreich, Vol. 23 (Academic Press, New York, 1969), p. 1.

[22] E. V. Chulkov, I. Sarría, V. M. Silkin, J. M. Pitarke, and P. M. Echenique, Phys. Rev. Lett. **80**, 4947 (1998).

[23] A. Eiguren, B. Hellsing, F. Reinert, G. Nicolay, E. V. Chulkov, V. M. Silkin, S. Hüfner, and P. M. Echenique, Phys. Rev. Lett. **88**, 066805 (2002).

[24] A. Eiguren, B. Hellsing, E. V. Chulkov, and P. M. Echenique, Phys. Rev. B **67**, 235423 (2003).

[25] M. Wiesenmayer, M. Bauer, S. Mathias, M. Wessendorf, E. V. Chulkov, V. M. Silkin, A. G. Borisov, J.-P. Gauyacq, P. M. Echenique, and M. Aeschlimann, Phys. Rev. B **78**, 245410 (2008).

[26] J. Graefenstein, I. Mertig, and R. Zeller, J. Phys. F **18**, 731 (1988).

[27] I. Mertig, E. Mrosan, and R. Schöpke, J. Phys. F **12**, 1689 (1982).

[28] A. C. Hewson, *The Kondo Problem to Heavy Fermions* (Cambridge Univrsity Press, Cambridge, UK, 2003).

[29] N. Papanikolaou, N. Stefanou, and C. Papastaikoudis, Phys. Rev. B **49**, 16117 (1994).

[30] P. Mavropoulos, N. Papanikolaou, and N. Stefanou, J. Phys.: Condens. Matter **7**, 4665 (1995).

[31] I. Mertig, Rep. Prog. Phys. **62**, 237 (1999).

[32] N. Papanikolaou, R. Zeller, and P. H. Dederichs, J. Phys.: Condens. Matter **14**, 2799 (2002).

[33] H. Ebert, D. Ködderitzsch, and J. Minar, Rep. Prog. Phys. **74**, 096501 (2011).

[34] K. Wildberger, R. Zeller, and P. H. Dederichs, Phys. Rev. B **55**, 10074 (1997).

[35] R. Zeller, P. H. Dederichs, B. Újfalussy, L. Szunyogh, and P. Weinberger, Phys. Rev. B **52**, 8807 (1995).

[36] S. Vosko, L. Wilk, and M. Nusair, Can. J. Phys. **58**, 1200 (1980).

[37] W. Shockley, Phys. Rev. **56**, 317 (1939).

[38] D. V. Fedorov, P. Zahn, M. Gradhand, and I. Mertig, Phys. Rev. B **77**, 092406 (2008).

[39] J. O. Linde, Ann. Phys. **402**, 52 (1931).

[40] J. O. Linde, Ann. Phys. **406**, 353 (1932).

[41] *Periodic Table of Elements* (Sargent-Welch Scientific, Buffalo Grove, IL, 1995).

[42] In photoemission spectroscopy, the surface state of silver is found to be 63 meV below the Fermi energy, while in Cu and Au. the surface states are much deeper in energy (435 and 484 meV below E_F).[5]

[43] S. S. Tsirkin, S. V. Eremeev, E. V. Chulkov, M. Marks, K. Schubert, J. Gdde, and U. Hfer, Phys. Rev. B **86**, 085424 (2012).

[44] J. Lobo-Checa, J. E. Ortega, A. Mascaraque, E. G. Michel, and E. E. Krasovskii, Phys. Rev. B **84**, 245419 (2011).

[45] R. Podloucky, R. Zeller, and P. H. Dederichs, Phys. Rev. B **22**, 5777 (1980).

[46] G. Grüner, Adv. Phys. **23**, 941 (1974).

[47] J. Cohen and C. Slichter, J. Appl. Phys. **49**, 1537 (1978).

[48] P. Coleridge, J. Phys. F **15**, 1727 (1985).

[49] R. Matzdorf, Chem. Phys. **251**, 151 (2000).